Hard-core bosons on optical superlattices: Dynamics and relaxation in the superfluid and insulating regimes

Marcos Rigol
Physics Department, University of California, Davis, California 95616, USA

Alejandro Muramatsu
Institut für Theoretische Physik III, Universität Stuttgart, Pfaffenwaldring 57, D-70550 Stuttgart, Germany

Maxim Olshanii
Department of Physics & Astronomy, University of Southern California, Los Angeles, California 90089, USA

We study the ground-state properties and nonequilibrium dynamics of hard-core bosons confined in one-dimensional lattices in the presence of an additional periodic potential (superlattice) and a harmonic trap. The dynamics is analyzed after a sudden switch-on or switch-off of the superlattice potential, which can bring the system into insulating or superfluid phases, respectively. A collapse and revival of the zero-momentum peak can be seen in the first case. We study in detail the relaxation of these integrable systems towards equilibrium. We show how after relaxation time averages of physical observables, like the momentum distribution function, can be predicted by means of a generalization of the Gibbs distribution.

PACS numbers: 03.75.Kk, 03.75.Hh, 05.30.Jp, 02.30.Ik

I. INTRODUCTION

In recent years the nonequilibrium dynamics of low-dimensional quantum systems has been increasingly attracting the attention of experimentalists and theoreticians from different areas of physics [1]. An exciting field in which great experimental progress has been achieved within the last decade is the one of ultracold quantum gases. There, advances in atom waveguide technology [2, 3, 4, 5, 6], the realization of quantum gases in very anisotropic traps [7, 8, 9], and loading Bose-Einstein condensates (BEC's) on optical lattices [10, 11, 12, 13, 14, 15, 16, 17] have allowed experimentalists to obtain a wide variety of systems in which the effects of the reduced dimensionality can be studied in detail.

Due to the very high control than can be achieved in an experiment with a degenerate quantum gas, one can prepare it under very specific initial conditions and study its evolution. This has been done in the one-dimensional (1D) regime in various experiments. For example, the transport properties of 1D Bose gases on a lattice have been studied in Refs. [12, 16], where the gas was displaced from the center of the trap and allowed to oscillate. More recently, Kinoshita *et al.* [17] have addressed experimentally the question of whether an isolated integrable or nearly integrable system can relax to the thermal equilibrium state [18].

On the theoretical side, integrability in low-dimensional systems allows one to perform exact studies of the equilibrium properties and the nonequilibrium dynamics of well-known models [19, 20, 21, 22, 23], some of which have already become relevant to experiments. One particular model in which we are interested in this work is the one of impenetrable bosons in 1D [14, 15, 17]. It has been shown theoretically [24, 25, 26] that in certain 1D regimes of low densities and low temperatures, bosons behave as a gas of impenetrable particles also known as Tonks-Girardeau bosons [hard-core bosons (HCB's)].

The 1D homogeneous gas of HCB's was introduced by Girardeau [27], who also established a one-to-one correspondence (Bose-Fermi mapping) between 1D HCB's and spinless fermions. This mapping has been recently used to study the nonequilibrium case [28, 29, 30, 31, 32], where the density dynamics revealed dark-soliton structures [28], breakdown of the time-dependent mean-field theory [29], interference patterns of the thermal gas on a ring [30], and other interesting effects during the expansion [31, 32].

Hard-core bosons have been also realized experimentally in the presence of a lattice along the 1D tubes [14]. In the periodic case, the HCB lattice Hamiltonian can be mapped onto the 1D XY model of Lieb, Schulz, and Mattis [33]. The 1D XY model has been extensively studied in the literature, and the asymptotic behavior of the correlation functions is known [34, 35, 36, 37]. With an additional confining potential, the case relevant to the experiments in Ref. [14], this model has been studied be means of an exact numerical approach in Ref. [38]. There it was shown that one-particle correlations exhibit a universal power-law decay. The generalization of the approach in Ref. [38] to the nonequilibrium dynamics [39, 40, 41] revealed that during the expansion of the HCB gas on the lattice two very different regimes can be identified. If the expansion starts from a Mott insulating state, quasi-long range correlations develop between initially uncorrelated particles, producing the emergence of quasicondensates at finite momentum [39, 41]. On the

other hand, for low initial densities (superfluid state), the momentum distribution of expanding HCB's rapidly approaches that of noninteracting fermions [40, 41].

In this work we study the nonequilibrium dynamics of hard-core bosons on 1D superlattices. The superlattice is obtained adding an extra periodic potential to the already existing lattice. In the soft-core regime these systems have been already realized experimentally [42, 43] and studied theoretically in 1D by various mean-field and perturbative approaches [44], quantum Monte Carlo simulations [45], and exact diagonalization [46]. In the hard-core regime, due to the mapping to noninteracting fermions, one can realize that the effect of the extra periodic potential is to open gaps at the boundaries of the reduced Brillouin zone. This means that in addition to the insulating phase with density 1 (full filling) new insulating phases appear at fractional fillings.

In three-dimensional systems the study of the half-filled hard-core boson model allowed one to prove rigorously the existence of Bose-Einstein condensation and Mott insulating phases tuning the strength of the additional lattice [47]. Here we quench the strength of the superlattice potential to study the dynamics of these systems in the superfluid and insulating regimes. We are interested in understanding how the system approaches equilibrium, if it does, and in testing the prediction power of a generalized Gibbs ensemble theory recently proposed in Ref. [18]. In order to do so, we also study the case in which an additional harmonic confining potential is introduced in the system, as relevant to most of the experimental situations. At low densities we obtain results similar to that of the recent experiment by Kinoshita *et al.* [17].

The exposition is organized as follows. In Sec. II we describe the ground-state properties of HCB's in a periodic superlattice, paying special attention to the behavior of the one-particle correlations in the superfluid and insulating regimes. Section III is devoted to the study of the nonequilibrium dynamics of the system after a sudden switch-on and -off of the superlattice potential—i.e., when going from the superfluid to the insulating phases and vice versa. Relaxation and the collapse and revival of the zero-momentum peak of the momentum distribution function are studied in detail. In Sec. IV we analyze the ground-state properties of the system in the presence of a trap, which produces a coexistence of superfluid and insulating phases. The nonequilibrium dynamics in the presence of a trap is studied in Sec. V. Finally, the conclusions are presented in Sec. VI.

II. HARD-CORE BOSONS IN PERIODIC SUPERLATTICES

The hard-core boson Hamiltonian in the presence of a superlattice potential can be written as

$$\hat{H} = -\sum_i \left(t_{i,i+1} \hat{b}_i^\dagger \hat{b}_{i+1} + \text{H.c.} \right) + A \sum_i \cos\left(\frac{2\pi i}{L}\right) \hat{n}_i, \tag{1}$$

where the HCB creation and annihilation operators at site i are denoted by $\hat{b}_i^\dagger$ and $\hat{b}_i$, respectively, and the local density operator by $\hat{n}_i = \hat{b}_i^\dagger \hat{b}_i$. In different sites the HCB creation and annihilation operators commute as usual for bosons:

$$[\hat{b}_i, \hat{b}_j^\dagger] = [\hat{b}_i, \hat{b}_j] = [\hat{b}_i^\dagger, \hat{b}_j^\dagger] = 0, \quad \text{for} \quad i \neq j. \tag{2}$$

However, on the same site these operators satisfy anti-commutation relations typical for fermions:

$$\left\{ \hat{b}_i, \hat{b}_i^\dagger \right\} = 1, \qquad \hat{b}_i^{\dagger 2} = \hat{b}_i^2 = 0. \tag{3}$$

These constraints avoid double or higher occupancy of the lattice sites. In Eq. (1), the hopping parameters are denoted by $t_{i,i+1} = t$. The last term represents the superlattice potential with strength A and unit cells with L sites.

Using the Jordan-Wigner transformation [48]

$$\hat{b}_i^\dagger = \hat{f}_i^\dagger \prod_{\beta=1}^{i-1} e^{-i\pi \hat{f}_\beta^\dagger \hat{f}_\beta}, \qquad \hat{b}_i = \prod_{\beta=1}^{i-1} e^{i\pi \hat{f}_\beta^\dagger \hat{f}_\beta} \hat{f}_i \ , \tag{4}$$

one can map the HCB Hamiltonian onto the one of non-interacting spinless fermions,

$$\hat{H}_F = -\sum_i \left(t'_{i,i+1} \hat{f}_i^\dagger \hat{f}_{i+1} + \text{H.c.} \right) + A \sum_i \cos\left(\frac{2\pi i}{L}\right) \hat{n}_i^f, \tag{5}$$

where $\hat{f}_i^\dagger$ and $\hat{f}_i$ are the creation and annihilation operators for spinless fermions at site i and $\hat{n}_i^f = \hat{f}_i^\dagger \hat{f}_i$ is the local particle number operator. Considering that

$$\hat{b}_N^\dagger \hat{b}_1 = -\hat{f}_N^\dagger \hat{f}_1 \ \exp\left(-i\pi \sum_{\beta=1}^{N} \hat{n}_\beta^f \right), \tag{6}$$

where N is the number of lattice sites, one notices that $t'_{N,1} = \exp\left[-i\pi(N_b+1)\right] t_{N,1}$; i.e., for periodic chains when the number of particles in the system ($N_b = \sum_i \langle \hat{n}_i \rangle = \sum_i \langle \hat{n}_i^f \rangle$) is odd, the equivalent fermionic Hamiltonian satisfies the same boundary conditions than the HCB one; otherwise, if N_b is even, the opposite boundary conditions are required for the fermionic Hamiltonian.

With the help of the mapping above one can realize that for HCB's in a superlattice insulating phases appear at fractional fillings ($n_i = i/L$, with $i = 1, \ldots, L-1$, unless a band crossing occurs [45]), in addition to the full

filling insulator ($n_i = 1$) already present in the absence of the superlattice. This is because in the equivalent system of noninteracting fermions the superlattice potential opens gaps at the boundaries of the reduced Brillouin zones. In what follows, for simplicity, we restrict our study to superlattices with $L = 2$. In this case the insulating phases occur at half and full filling. The generalization of our results to larger values of L is straightforward, and does not (qualitatively) change the results we discuss for $L = 2$.

In order to study the bosonic one-particle correlations

$$\rho_{ij} = \left\langle \hat{b}_i^\dagger \hat{b}_j \right\rangle \tag{7}$$

and related quantities like the momentum distribution function

$$n_k = \frac{1}{N} \sum_{jl} e^{-ik(j-l)} \rho_{jl}, \tag{8}$$

we follow the exact approach described in detail in Ref. [38]. This approach allows us to study very large system sizes (thousands of lattice sites) in a very efficient way.

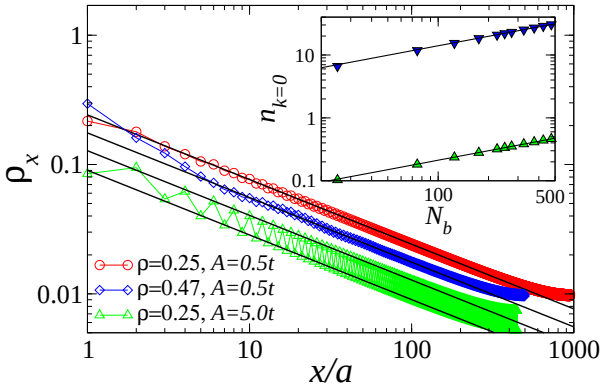

FIG. 1: (Color online) Decay of one-particle correlations (averaged per unit cell as described in the text) in the superfluid phase. These systems have up to 1900 lattice sites and $L = 2$. The plot for $\rho = 0.25$, $A = 5t$ was displaced down for clarity. Straight solid lines correspond to power laws $1/\sqrt{x}$. The inset shows $n_{k=0}$ (top) and $n_{k=\pm\pi/a}$ (bottom) vs N_b for systems at quarter filling and $A = 0.5t$. The straight lines signal $\sqrt{N_b}$ behavior. Distances are normalized by the lattice constant a.

In Fig. 1 we show how the one-particle correlations decay in the presence of a superlattice potential in the superfluid phase. In the figure we have averaged the correlations measured from the even and odd sites in order to minimize the effects of the different density in the sites; i.e., we have plotted

$$\rho_x = \frac{1}{2}\left(\rho_{i^{odd},i^{odd}+x/a} + \rho_{i^{even},i^{even}+x/a}\right).$$

As can be seen in Fig. 1, one-particle correlations in the superlattice decay with the same power law $\rho_x \sim 1/\sqrt{x}$ that was shown to be universal in absence of the superlattice potential [38]. The only effect that the superlattice introduces and that is evident only for large values of A is an oscillatory behavior in ρ_x on top of the $1/\sqrt{x}$ decay.

The existence of quasi-long-range one-particle correlations implies that, like in the usual lattice, a sharp peak in the momentum distribution function at $k = 0$ signals the superfluid state. The additional oscillatory behavior seen in ρ_x (Fig. 1) is reflected by additional peaks in n_k at $ka = \pm\pi$, which deplete the one in $k = 0$ from its value for $A = 0$. This can be seen in Figs. 2(a) and 2(c), where we have plotted the momentum distribution function for two different values of the strength of the superlattice potential. A simple calculation also allows to extract from $\rho_x \sim 1/\sqrt{x}$ the scaling behavior of the $k = 0$ and $k = \pm\pi/a$ peaks as the system size is increased keeping the density constant. One finds that $n_{k=0,\pm\pi/a} \sim \sqrt{N_b}$. Such scaling can be seen in the inset of Fig. 1 where we have plotted these quantities for systems at quarter filling and $A = 0.5t$.

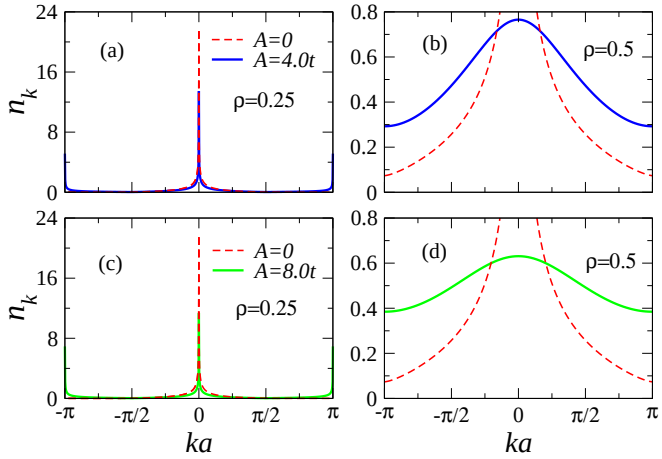

FIG. 2: (Color online) Momentum profiles for periodic systems with 900 lattice sites in a superlattice potential with $L = 2$. In (a) and (c) the system is in a superfluid state. The peaks at $k = 0$ and $k = \pm\pi/a$ signal the presence of quasi-long range one-particle correlations (Fig. 1). On the other hand, in (b) and (d) the system is in an insulating state where one-particle correlations decay exponentially (Fig. 3).

At half filling the behavior of the system is completely different to the one above. As mentioned before a gap opens in the spectrum. Since Eq. (5) can be easily diagonalized for $L = 2$, one immediately obtains that the gap is $\Delta = 2A$, and the dispersion relation in the two bands is

$$\epsilon_\pm(k) = \pm\sqrt{4t^2\cos^2(ka) + A^2}, \tag{9}$$

where by "+" we mean the upper band and by "−" the lower one.

The presence of this gap produces an exponential decay of the one-particle correlations as shown in Fig. 3. The correlation length ξ is a function of the gap—i.e., of A. We have calculated the correlation length ξ as the second

moment of the one-particle density matrix,

$$\xi = \sqrt{\frac{1}{2}\frac{\sum_{ij}(x_i - x_j)^2 \rho_{ij}}{\sum_{ij}\rho_{ij}}}, \tag{10}$$

which for large values of ξ is equivalent to calculating it fitting an exponential decay $\rho_x \sim \exp(-x/\xi)$, as shown at finite temperatures in Ref. [49].

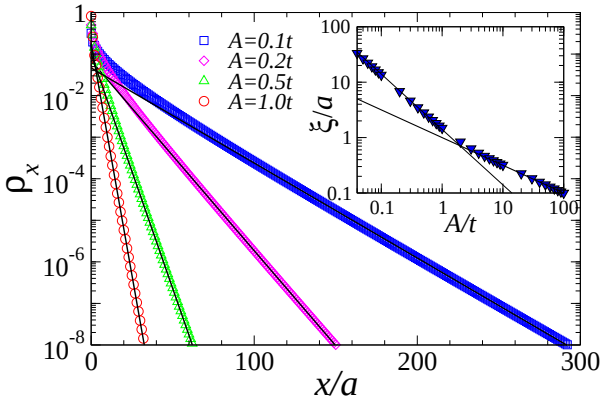

FIG. 3: (Color online) Decay of one-particle correlations (averaged per unit cell as described in the text) in the insulating (half-filled) case. The systems considered have up to 1500 lattice sites and $L = 2$. The straight lines signal an exponential decay with a correlation length ξ, which is a function of A. In the inset we show ξ vs A. The straight lines depict the asymptotic behavior of ξ. For very small values of A one has that $\xi/a \sim 1/(A/t)$ while for large values of A one obtains that $\xi/a \sim 1/\sqrt{A/t}$ (where a is the lattice constant).

The behavior of ξ as a function of A is shown in the inset of Fig. 3. There one can see that it exhibits two different functional forms for small and large values of A. For small values of A we find that $\xi/a \sim 1/(A/t)$, while for large values of A it is $\xi/a \sim 1/\sqrt{A/t}$ (a is the lattice constant). In general, a correlation length $\xi \sim 1/A$ develops from free bosonic excitations across a gap $\sim A$. Such an argument results already at a mean-field level, and in the absence of diverging correlation lengths, it is qualitatively correct for small values of A. For very large values of A one can use perturbation theory to determine the asymptotic behavior of ξ. For $A/t \to \infty$ the ground state at half filling is just an array of Fock states with one particle in the odd sites and no particle in the even sites $|\Psi\rangle_{A/t\to\infty} = \prod_i |1\rangle_{i_{odd}}|0\rangle_{i_{even}}$. Up to first order in perturbation theory the ground state of the system can be written as

$$|\Psi\rangle_G \approx |\Psi\rangle_{A/t\to\infty} + \frac{t}{2A}\sum_i \left(\hat{b}_i^\dagger \hat{b}_{i+1} + \text{H.c.}\right)|\Psi\rangle_{A/t\to\infty}, \tag{11}$$

which means that for $i \neq j$ [the only ones that contribute to the numerator in Eq. (10)]

$$\begin{aligned} \rho_{ij} = \langle \hat{b}_i^\dagger \hat{b}_j \rangle_G &= \frac{t}{2A} \quad \text{for} \quad |i-j| = 1, \\ &= 0 \quad \text{for} \quad |i-j| > 1. \end{aligned} \tag{12}$$

In the denominator in Eq. (10) only the terms $i = j$ (the densities) contribute to first order. Hence,

$$\xi = a\sqrt{\frac{t}{A}} \tag{13}$$

for very large values of A/t. Indeed, $\xi/a = \sqrt{t/A}$ is the straight line that in the inset in Fig. 3 follows the data points for large values of A.

The consequence of the exponential decay of the one-particle correlations in the momentum distribution function can be seen in Figs. 2(b) and 2(d). There we have plotted n_k for two different values of A and compared it with $A = 0$. The effect of the gap at half filling is dramatic. It destroys the peaks in the momentum distribution function. This feature can be used experimentally to detect the presence of an insulating state in a superlattice, like it has been done previously to detect the presence of a Mott insulator in the absence of the superlattice.

An overall picture of the behavior of the momentum distribution function when changing the density can be obtained plotting $n_{k=0}$ vs ρ as shown in Fig. 4. For contrast we have also plotted the result for $A = 0$. Figure 4 shows that while for low densities the effect of A is almost imperceptible, it becomes very large as the density approaches half filling. In the insulating state $n_{k=0}$ attains its minimum value.

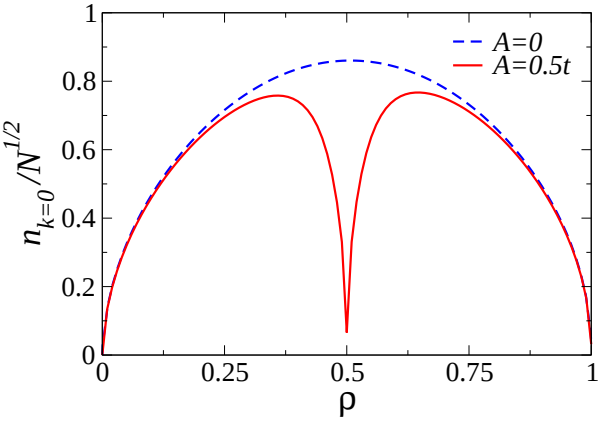

FIG. 4: (Color online) Normalized occupation of the $k = 0$ momentum state as a function of the density in periodic systems with $N = 1000$. For $A \neq 0$ one can see that $n_{k=0}$ is strongly suppressed around $n = 0.5$, where the system is an insulator.

III. DYNAMICS AND RELAXATION IN THE SUPERFLUID AND INSULATING REGIMES

We study in this section the dynamics of hard-core bosons on superlattices when by a sudden change of the strength of the superlattice potential one goes from a superfluid to an insulating regime, and vice versa. Since for $L = 2$ this can only occur at half filling, we will restrict

our analysis to that case. In addition, for a closer connection with the experiments instead of periodic systems we consider open boxes, where translational invariance is broken, but keeping the same phase diagram than in the periodic case. We will consider systems confined in harmonic traps, where superfluid and insulating phases can coexist, in the next two sections.

We start our study with the case in which the initial state is superfluid, at half filling with $A = 0$, and A is suddenly changed to a finite value, for which in the ground state the system would be an insulator. This is similar, in the Hubbard model, to a change of the on-site repulsion U from a value in which the system is superfluid to $U > U_c$ (U_c being the critical value for the formation of a Mott insulator). The number of particles per site in this case has to be integer. Such study for a Hubbard like experimental system has been done in three-dimensional optical lattices in Ref. [50].

In the experiment [50] it was found that as the system evolves a collapse and revival of the initial momentum distribution function (the interference pattern) occurs. This can be easily understood considering that for time scales much smaller than the one set by the hopping parameter, the particle number per lattice site remains almost unchanged and only the phases evolve. This evolution is dictated by the on-site interaction between atoms (U), which in the Hubbard language reads

$$\hat{H}_{int} = \frac{1}{2} U \hat{n}(\hat{n} - 1). \tag{14}$$

Hence, the evolution operator has the form $\exp[-iUn(n-1)\tau/2]$, where τ is a time variable (which we will give in units of $\hbar$ in what follows). This means that phases in different lattices sites evolve differently, according to the number of atoms present, collapsing the interference pattern. However, for times $\tau_{rev} = 2\pi n/U$, where n is an integer, a revival of the interference pattern occurs.

In Fig. 5 we show the time evolution of the occupation of the zero-momentum state for a box that initially has $A = 0$ and the evolution is performed by a sudden change to three different values of the final A. This figure shows that also in a 1D superlattice loaded with HCB's a collapse and revival of the zero-momentum peak occurs. Here, double or higher occupancy is forbidden by the hard-core constraint ($U = \infty$) so that the short-time evolution is only determined by the term in the Hamiltonian proportional to the superlattice potential,

$$\hat{H} = A \sum_i (-1)^i \hat{n}_i, \tag{15}$$

which means that A is the parameter that controls the revival time (equivalent to U in the Hubbard case). This can be better seen in the insets in Fig. 5, where we have plotted the first three revivals of $n_{k=0}$. Comparing the times with the values of A one can see that indeed $\tau_{rev} \sim \pi n/A$.

The second effect that is apparent in Fig. 5 is the damping of the collapse and revival of the zero-momentum peak of n_k. It is related to the change of

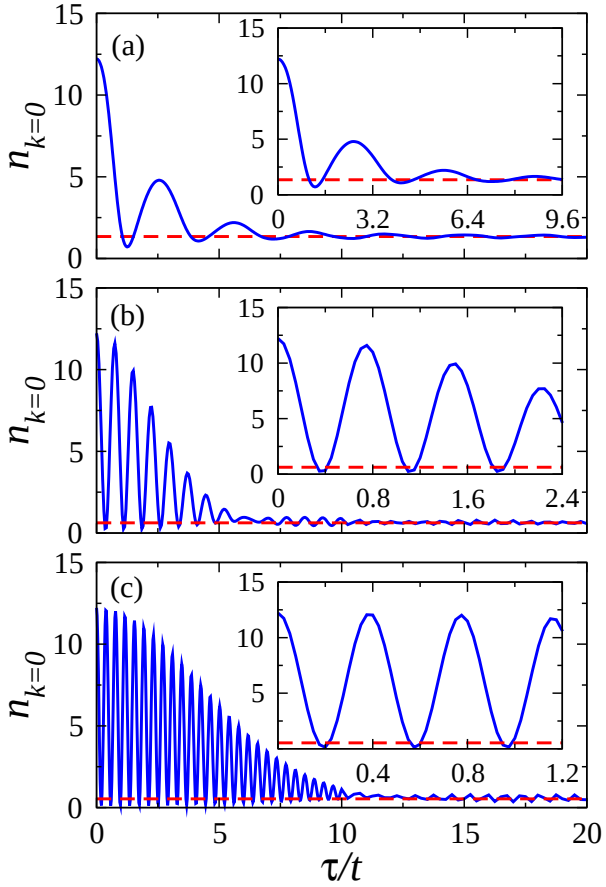

FIG. 5: (Color online) Evolution of the occupation of the zero-momentum state after A is changed from $A = 0$ in the initial (superfluid) state to $A = 1.0t$ (a), $A = 4.0t$ (b), and $A = 8.0t$ (c). The insets show in more detail the first three revivals of $n_{k=0}$. Dashed lines show $n_{k=0}$ obtained from the constrained thermodynamics theory (see text). These systems have 300 lattice sites, 150 particles, and $L = 2$.

the occupation of each lattice site due to the finite value of the hopping parameter t. Variations in the density destroy the periodic evolution set by Eq. (15). In these systems the dynamics of the density is determined by a combination of the times scales given by t and A. (Notice that A in the even sites acts like a barrier between odd sites.) In Fig. 5 one can see that the largest damping occurs for the smallest the value of A/t. For the largest value of A shown in the figure ($A = 8t$) the collapse and revival is almost completely damped after $\tau = 10t$.

After observing the damping of the collapse and revival of the momentum distribution function in Fig. 5 one immediate question one could ask is to what kind of momentum distribution is the system relaxing. In nonintegrable systems one expects n_k to relax to the thermal distribution. In the grand canonical ensemble it can be obtained using the many-body density matrix

$$\hat{\rho} = Z^{-1} \exp\left[-\left(\hat{H} - \mu \hat{N}_b\right)/k_B T\right], \tag{16}$$

where

$$Z = \mathrm{Tr}\left\{\exp\left[-\left(\hat{H} - \mu\hat{N}_b\right)/k_BT\right]\right\} \tag{17}$$

is the partition function. In order to determine the relevant temperature (k_BT) and the chemical potential (μ) one can use the energy and number of particles of the evolving system, which do not change during the dynamics; i.e., k_BT and μ can be calculated using the constraints

$$E = \mathrm{Tr}\left[\hat{H}\hat{\rho}\right], \quad N_b = \mathrm{Tr}\left[\hat{N}_b\hat{\rho}\right]. \tag{18}$$

In Fig. 6 we compare the momentum distribution function obtained within the grand-canonical approach described above (called "thermal" in the figure) with the time-averaged momentum distribution obtained during the evolution, after the damping of the oscillations shown in Fig. 5. We have averaged the time evolving $n_k(\tau)$ because, as can be seen in Fig. 5, this quantity exhibits fluctuations around its mean value. The exact n_k's for the thermal equilibrium were obtained using the method detailed in Ref. [49]. Figure 6 clearly shows that the mean values around which $n_k(\tau)$ fluctuates are not the ones of the usual thermal equilibrium; i.e., these systems are not ergodic in the usual sense. Since hard-core bosons in 1D lattices are integrable [33], nonergodic behavior may have been expected due to the presence of extra constants of the motion (whose number is infinite in the thermodynamic limit) in addition to the energy and the number of particles.

The problem of relaxation in an integrable system, like the one of hard-core bosons that we are analyzing here, has been already discussed in Ref. [18]. There it was conjectured that the correct many-body density matrix that describes the properties of an integrable system after relaxation is given by a generalization of the Gibbs ensemble

$$\hat{\rho}_c = Z_c^{-1}\exp\left(-\sum_m \lambda_m \hat{I}_m\right), \tag{19}$$

where

$$Z_c = \mathrm{Tr}\left[\exp\left(-\sum_m \lambda_m \hat{I}_m\right)\right] \tag{20}$$

is the corresponding partition function, $\{I_m\}$ is a full set of integrals of motion, $\{\lambda_m\}$ are the Lagrange multipliers, and $m = 1, \ldots, N$. These Lagrange multipliers can be calculated using the expectation values of the full set of integrals of motion of the evolving system, which do not change with time

$$\langle \hat{I}_m \rangle_\tau = \mathrm{Tr}\left[\hat{I}_m\hat{\rho}_c\right]. \tag{21}$$

In Eq. (21) and in what follows, $\langle\cdots\rangle_\tau$ means expectation values in the time-evolving system when they do not depend on time.

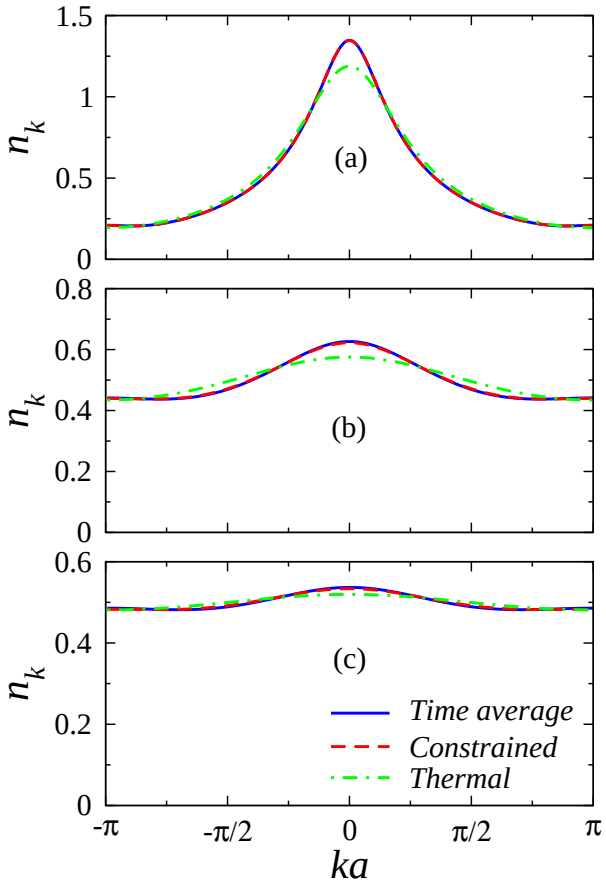

FIG. 6: (Color online) Time average of the momentum distribution function after the damping of the oscillations seen in Fig. 5. We averaged measurements done in time intervals $\Delta\tau = 20t$ between times $\tau = 20t$ and $\tau = 5000t$. The time average is compared with the results obtained in the usual thermal ensemble and the constrained theory explained in the text. These systems have 300 lattice sites, 150 particles, and $L = 2$. In all cases the initial $A = 0$ and the final one $A = 1.0t$ (a), $A = 4.0t$ (b), and $A = 8.0t$ (c). The corresponding temperatures in the grand-canonical ensemble are $k_BT = 0.86t$ (a), $k_BT = 6.86t$ (b), and $k_BT = 25.75t$ (c).

The conjecture above is still based on the ergodic hypothesis, but generalized to consider that the region available of phase space is determined by *all* constants of the motion, and not only by E and N as usual for nonintegrable systems. Hence, what the density matrix defined by Eq. (19) does is to maximize the many body Gibbs entropy,

$$S = k_B\mathrm{Tr}\left[\hat{\rho}_c \ln\left(\frac{1}{\hat{\rho}_c}\right)\right], \tag{22}$$

subject to the constraints imposed by all the integrals of motion.

Like in the ground state [38] and the thermal equilibrium case [49], in order to calculate the HCB expectation values using Eq. (19) we take advantage of the Jordan-Wigner transformation and the mapping to noninteracting fermions. In fermionic language the integrals

of motion can be easily constructed after diagonalizing the Hamiltonian (5):

$$\hat{H}_F \hat{\gamma}_m^{f\dagger}|0\rangle = E_m \hat{\gamma}_m^{f\dagger}|0\rangle. \quad (23)$$

Since the occupation of the eigenstates of the final fermionic Hamiltonian cannot change in time, these fermions are noninteracting; a complete set of integrals of motion can be constructed to be

$$\left\{\hat{I}_m^f\right\} = \left\{\hat{\gamma}_m^{f\dagger}\hat{\gamma}_m^f\right\}. \quad (24)$$

The constraints in Eq. (20), in the fermionic representation, lead to an analytical expression for the Lagrange multipliers,

$$\lambda_m = \ln\left(\frac{1-\langle\hat{I}_m^f\rangle_\tau}{\langle\hat{I}_m^f\rangle_\tau}\right), \quad (25)$$

which allows us to build the equivalent fermionic Hamiltonian and to obtain the HCB expectation values using the approach explained in detail in Ref. [49]. One should notice at this point that the constraints defined by Eq. (24), when written in the bosonic language, involve many bosonic creation and annihilation operators. Hence, these constraints lose the bilinear character they have in the fermionic representation.

In Fig. 6 one can see that the results obtained with the constrained thermodynamics theory explained above are indistinguishable from the ones of the time average after damping. Hence, even for the evolution of these pure quantum states in integrable systems one can define a constrained ensemble able to predict the mean values of observables after relaxation. We have also included in Fig. 5 the value of $n_{k=0}$ obtained from the constrained thermodynamic theory for a comparison with the time evolving $n_{k=0}(\tau)$. There one can see that after relaxation the small fluctuations of $n_{k=0}(\tau)$ indeed occur around the value obtained with the generalized Gibbs ensemble. Notice that the case described so far in this section seems to be one of the worst scenarios for HCB's since the evolution is performed with a Hamiltonian for which the ground state of the system is gapped; i.e., relaxation is expected to occur slowly due to the presence of the gap.

In what follows we consider the inverse case. The case in which initially the system is in an insulating state and by turning off the superlattice potential this state is allowed to evolve with a Hamiltonian whose ground state is superfluid.

In Fig. 7, we show the time evolution of $n_{k=0}$ from three initial insulating states. They have the same values of A used during the evolution of the systems in Figs. 5 and 6. The evolution is performed after turning off the superlattice potential (making $A = 0$). In contrast to the case in which the superlattice is turned on, one can

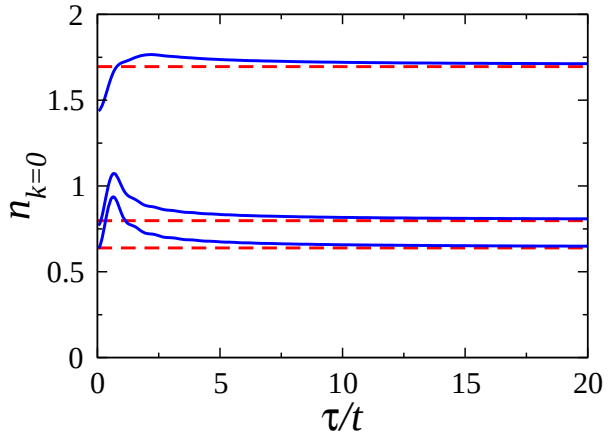

FIG. 7: (Color online) Evolution of the occupation of the zero-momentum state after A is changed from $A = 1.0t$, $A = 4.0t$, and $A = 8.0t$, (from top to bottom) in the initial (insulating) state to $A = 0$. Dashed lines show $n_{k=0}$ obtained from the constrained thermodynamics theory (see text). These systems have 300 lattice sites, 150 particles, and $L = 2$.

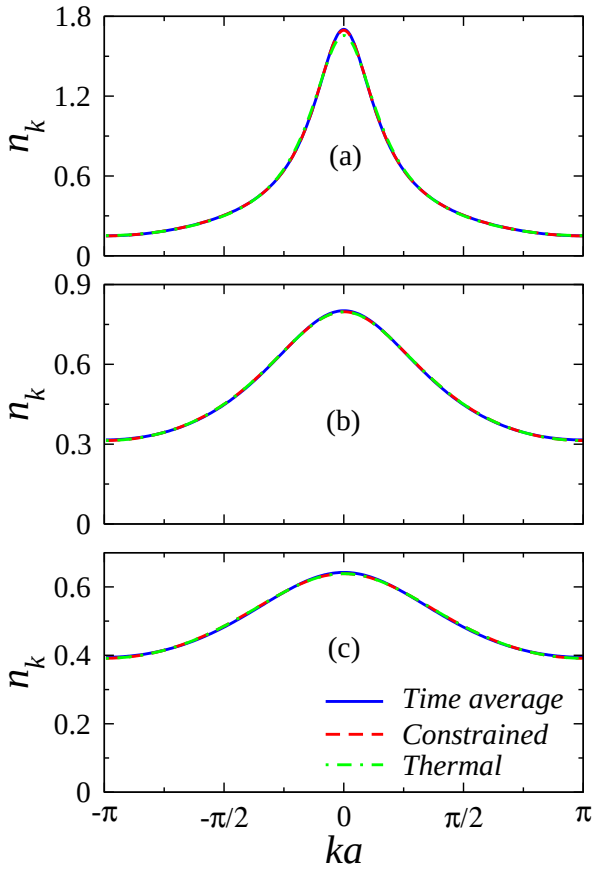

FIG. 8: (Color online) Time average of the momentum distribution function measured in time intervals $\Delta\tau = 20t$ between times $\tau = 20t$ and $\tau = 5000t$. The time average is compared with the results obtained in the usual thermal ensemble and the constrained theory explained in the text. These systems have 300 lattice sites, 150 particles, and $L = 2$. Initially $A = 1.0t$ (a), $A = 4.0t$ (b), and $A = 8.0t$ (c), and in all cases the final value of A is $A = 0$. The corresponding temperatures in the grand-canonical ensemble are $k_BT = 0.63t$ (a), $k_BT = 2.06t$ (b), and $k_BT = 4.03t$ (c).

see in Fig. 7 that no collapse and revivals occur in n_k. After an increase of the occupation of $n_{k=0}$ the system steadily relaxes to an approximately constant momentum distribution.

As before, in Fig. 8 we compare the results of the time average of the momentum distribution function after the system has relaxed to a stationary distribution with the expectation values of this quantity in the grand-canonical ("thermal" in the figure) and generalized ("constrained" in the figure) Gibbs ensemble. Remarkably, when one starts from an insulating state, where correlations decay exponentially—i.e., there is no quasi-long-range order—the results obtained within a grand-canonical description are very similar to the ones obtained during the time evolution. As can be seen comparing Figs. 8(a), 8(b), and 8(c), the deeper the initial state is in the insulating regime the better is the agreement between the grand-canonical and the average of the time evolving n_k's after. Actually, only in Fig. 8(a) can one clearly distinguish the differences in the occupation of the momentum states with very low values of k. On the other hand, the results obtained within the constrained theory are in all cases indistinguishable from the ones obtained during the time evolution.

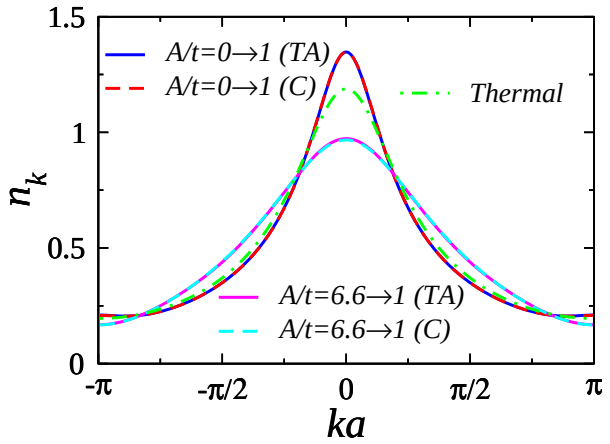

FIG. 9: (Color online) Comparison between the time average of the momentum distribution function of two systems starting from different initial conditions but having the same energy during the evolution. (As in the previous figures, n_k for the time average was measured in intervals $\Delta\tau = 20t$ between times $\tau = 20t$ and $\tau = 5000t$.) In both cases the evolution is done with a Hamiltonian in which $A = 1.0t$, but the initial state is in one case a superfluid state ($A = 0$), and in the other an insulating state with $A = 6.6t$. The time average is compared with the results obtained in the usual thermal ensemble (which depends only on the final energy and the number of particles—i.e., is the same in both cases) and the constrained theory explained in the text. These systems have 300 lattice sites, 150 particles, and $L = 2$. In the legend "(TA)" means time average in the out-of-equilibrium system and "(C)" the result of the constrained thermodynamics.

A further proof of the "memory" that these integrable systems have on the initial conditions can be obtained comparing the final momentum distribution function to which the system relaxes starting from two different initial states that have the same final energy. This comparison is done in Fig. 9 where we show results for two systems that start their evolution from a supperfluid (zero A) and insulating (nonzero A) states, evolving with a Hamiltonian in which the ground state is an insulator (nonzero A). While the usual grand-canonical description anticipates that they both should relax to the same momentum distribution, it can be seen in the figure that this is not the case. Only the generalized Gibbs distribution introduced before predicts two final momentum distribution functions and hence is able to describe the mean values of n_k after relaxation.

To conclude this section we would like to make some remarks about the one-particle density matrix. While in the usual and generalized Gibbs distributions one can easily work in a basis where this quantity is real, this is not the case during the nonequilibrium dynamics of a quantum system. In the latter case, in all our calculations, the one-particle density matrix is a complex object ($\rho_x(\tau) = |\rho_x(\tau)| \exp[-i\theta_x(\tau)]$) and nontrivial time-dependent phases $[\theta_x(\tau)]$ enter into play. An example in which these phases play a fundamental role was mentioned in the Introduction. In Ref. [40] it was shown that during the free expansion of the hard-core boson gas on a lattice n_k approaches the one of noninteracting fermions. This occurs due to the effects of $\theta_x(\tau)$ since $|\rho_x(\tau)|$ was found to decay with exactly the same power law than in equilibrium, which would mean that the system should have a large peak at $k = 0$.

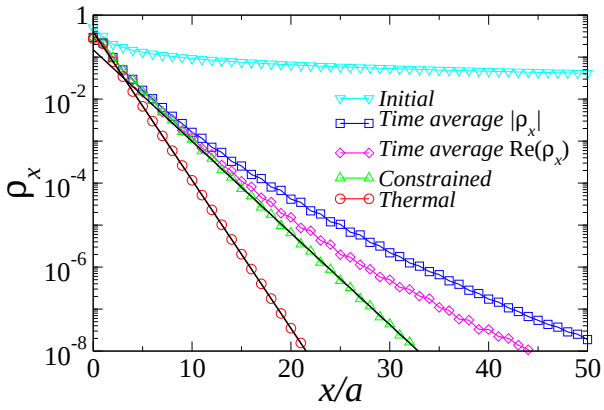

FIG. 10: (Color online) Time average of the modulus and real part of the one-particle density matrix compared with the power-law decay present in the initial state and with the results obtained using the usual (thermal) and generalized (constrained) Gibbs distributions. We calculated ρ_x from the center of the box, and for the time average we measured ρ_x in time intervals $\Delta\tau = 20t$ between $\tau = 20t$ and $\tau = 5000t$. These systems have 300 lattice sites, 150 particles, and $L = 2$. The initial value of A is $A = 0$ and the final one $A = 1.0t$. Straight lines following the constrained and thermal results signal an exponential decay of ρ_x.

We find that after relaxation both the modulus and the real part of the one-particle density matrix in the time evolving system are very different from ρ_x in the

thermal and constrained ensemble, for large values of x. This can be seen in Fig. 10 where we have plotted time average and thermodynamic results. [We did not include results for $\mathrm{Im}(\rho_x)$ since it oscillates strongly between positive and negative values.] Figure 10 shows that while in the usual and generalized Gibbs ensemble one-particle correlations decay exponentially at large distances (with different correlation lengths in each case), no such simple exponential decay can be seen either in the modulus or the real part of ρ_x in the evolving system. In addition, the decay of the correlations in the latter case cannot be described by a power law like the one in the initial state. Their decay is actually faster. (We also show in the figure ρ_x in the initial superfluid state.) The nontrivial effect of the phases $\theta_x(\tau)$ is evident in n_k, which is the diagonal part of the Fourier transform of the one-particle density matrix. While the mean value of $|\rho_x|$ in the out-of-equilibrium system decays more slowly than ρ_x in the constrained thermodynamics, the n_k obtained from both of them are identical [Fig. 6(a)]. We then conclude that there is no simple comparison possible between the time average of one-particle correlations in the system out of equilibrium (after relaxation) and in its "equivalent" generalized Gibb's ensemble. Hence, we do not consider that this quantity, which is not a physical observable, is an indicator of thermalization.

IV. HCB'S IN A SUPERLATTICE PLUS A HARMONIC CONFINING POTENTIAL

In this, and the following section, we generalize the results obtained in the previous sections to inhomogeneous systems. In particular, we study the effects of having a harmonic confining potential, relevant to experimental systems, in addition to the superlattice potential. In this case the Hamiltonian reads

$$H = -\sum_i \left(t_{i,i+1} b_i^\dagger b_{i+1} + \mathrm{H.c.}\right) + A\sum_i \cos\left(\frac{2\pi i}{L}\right) n_i + V_2 \sum_i x_i^2\, n_i, \tag{26}$$

where V_2 is the curvature of the harmonic trap. As in the previous sections in what follows we restrict the analysis to the case $L = 2$.

From earlier studies of the bosonic Hubbard model in a trap it is known that in the presence of a confining potential superfluid and Mott-insulating phases coexist space separated [51, 52, 53]. On the other hand, in the HCB case it has been shown that the presence of the trap does not destroy the power-law decay of the one-particle correlations known from the homogeneous case [38].

Previous studies have shown that the key parameter that controls the thermodynamic behavior of these confined systems is the characteristic density

$$\tilde{\rho} = N_b/\zeta, \tag{27}$$

where $\zeta = (V_2/t)^{-1/2}$ is a length scale set by the combination of the trap and the underlying lattice [38]. As $\tilde{\rho} \to 0$, one recovers the continuum limit. On the other hand, as $\tilde{\rho}$ increases beyond a critical value insulating regions build up in the system. In what follows we normalize distances in the trap by ζ and calculate the momentum distribution function as

$$n_k = \frac{a}{\zeta}\sum_{jl} e^{-ik(j-l)}\rho_{jl}. \tag{28}$$

In Figs. 11(a)–11(d) we show the density profiles (averaged per unit cell) for harmonically trapped systems with $A = 0.5t$, at different fillings. These plots show that like in the Bose-Hubbard case superfluid and insulating (constant density $n = 0.5$ and 1) phases coexist space separated in the trap. The width of the insulating phases with $n = 0.5$ is determined by the gap, which for the cases depicted in Fig. 11 is $\Delta = t$. The effect of the curvature of the harmonic potential is already considered by normalizing the distances by ζ.

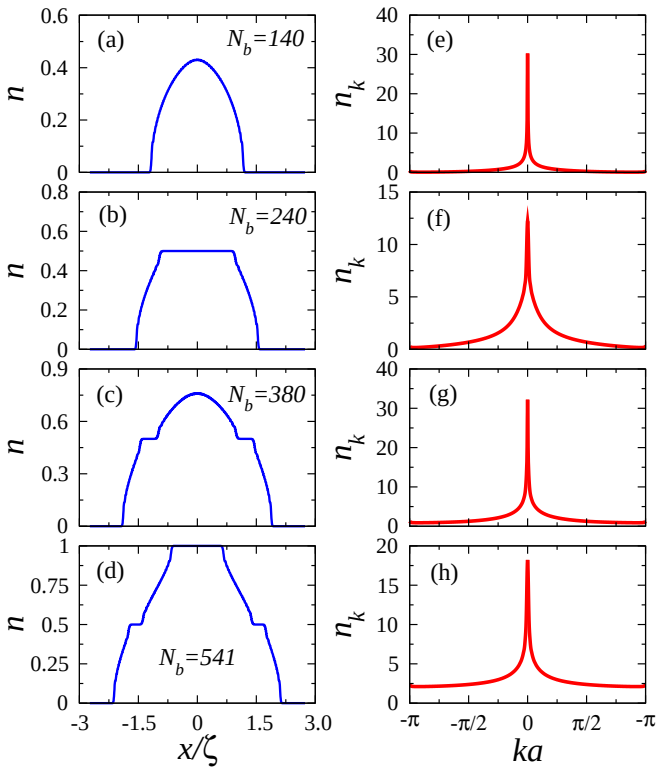

FIG. 11: (Color online) Density (averaged per unit cell) (a)–(d) and normalized momentum distribution function (e)–(h) for trapped systems with 1000 lattice sites, $V_2a^2 = 3\times10^{-5}t$, $L = 2$, and $A = 0.5t$. In (a)–(d), the regions with constant density are local insulators.

The formation of insulating domains in the trap strongly supresses the peaks observed in the momentum distribution at $k = 0$. This can be seen in Figs. 11(e)–11(h), where we have plotted the momentum profiles corresponding to the densities in Figs. 11(a)–11(d). However, these peaks are not destroyed and can be very

sharp. As can be seen in Fig. 12, the reason is that quasi-long-range correlations are still present in the superfluid regions. We find that their power-law decay is the same observed in the absence of the superlattice [38] and in the periodic case discussed in Sec. II—i.e., $\rho_x \sim 1/\sqrt{x}$, with $x = |x_i - x_j|$. Here of course translational invariance is broken by the trap; however, the above power law can be seen independently of the points x_i and x_j chosen within the superfluid part. On the other hand, as expected, in the insulating phases, where the density is constant, the decay of ρ_x is exponential, exactly like the one in Fig. 3. The particles there, being localized, are the ones that mainly contribute to the high momentum tails of n_k.

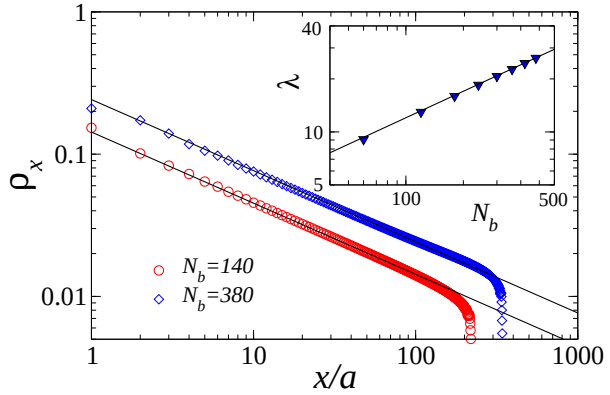

FIG. 12: (Color online) Decay of one-particle correlations ρ_x ($x = |x_i - x_j|$) (averaged per unit cell as described in Sec. II) in the superfluid domains. We have chosen x_i to be the center of the trap [see the corresponding density profiles in Figs. 11(a) and 11(c)]. Straight lines signal a power-law decay $\rho_x \sim 1/\sqrt{x}$, which disappears when $n_j \to 0$, 0.5, or 1. In the inset we show the scaling of the lowest natural orbital occupation with an increasing number of particles keeping constant the characteristic density of the system, which in this case is $\tilde{\rho} = 0.66$. The straight line shows that $\lambda_0 \sim \sqrt{N_b}$.

More information about the physics of the trapped system can be obtained studying the natural orbitals (ϕ^η), which can be considered to be like effective single-particle states when the system consists of interacting particles. They are defined as the eigenfunctions of the one-particle density matrix ρ_{ij} [54],

$$\sum_{j=1}^{N} \rho_{ij} \phi_j^\eta = \lambda_\eta \phi_i^\eta. \tag{29}$$

λ_η denotes the occupation of each orbital. In higher dimensions, when only the lowest natural orbital (the highest occupied one) scales $\sim N_b$, it can be regarded as the BEC order parameter—i.e., the condensate [55]. This scaling of the lowest natural orbital in higher dimensions is related to the presence of long-range off-diagonal order [56]. In the one-dimensional case we are studying here there is no long-range order, only quasi-long-range order characterized by a $1/\sqrt{x}$ decay of the correlations (Fig. 12), which as shown in the inset of Fig. 12 produces a power-law ($\sqrt{N_b}$) scaling of the lowest natural orbital occupation. (These scaling laws have also been observed in harmonically trapped continuous systems [57, 58, 59].) Hence, we refer to the lowest natural orbital as a quasicondensate since $\lambda_0 \to \infty$ when $N_b \to \infty$, but $\lambda_0/N_b \to 0$.

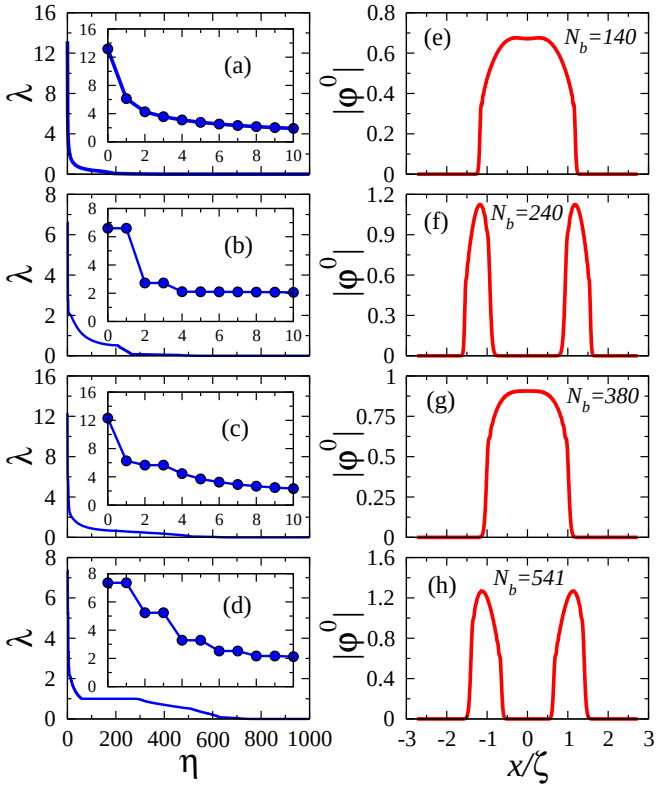

FIG. 13: (Color online) Natural orbital occupations (a)–(d) and normalized wave function of the lower natural orbital $\varphi^0 = (N_b\zeta/a)^{1/4}\,\phi^0$ (averaged per unit cell) (e)–(h), for trapped systems with 1000 lattice sites, $V_2a^2 = 3 \times 10^{-5}t$, $L = 2$, and $A = 0.5t$. In the insets of (a)–(d) we show the occupation of the lowest 11 natural orbitals, where degeneracy can be seen in the presence of the insulating domains. Comparing (e)–(h) with Figs. 11(a)–11(d) one can see that the lowest natural orbitals only have a finite weight in the superfluid domains.

In Figs. 13(a)–13(d) we show the occupation of the natural orbitals (ordered from the highest occupied one to the lowest occupied one) as a function of the orbital number η. The formation of the insulating domains not only reduces the occupation of the lowest natural orbitals, but also makes them degenerate (insets). The normalized wave function of the lowest natural orbitals [38]

$$\varphi^0 = (N_b\zeta/a)^{1/4}\,\phi^0, \tag{30}$$

are plotted in Figs. 13(e)–13(h). Comparing these wave functions with the density profiles in Figs. 11(a)–11(d) one can see that these orbitals are localized in the superfluid regions and have zero weight in the insulating domains. Degeneracy then appears because two identical quasicondensates develop to the sides of the central insulating core in the cases depicted in Figs. 11(b) and 11(d).

According to the number of particles in the system the lowest natural orbitals can be located outside or inside the insulating domains with average density $n = 0.5$.

The behavior of the lowest natural orbital occupations with an increasing number of particles in the trap can be seen in Fig. 14. It perfectly reflects the formation and destruction of insulating domains in the system. The first degeneracy for the four lowest natural orbitals (Fig. 14) appear when the insulating phase with mean density $n = 0.5$ sets in the middle of the trap [Fig. 11(b)]. This degeneracy disappears for the natural orbitals 3 and 4 when a superfluid domain, like the one in Fig. 11(c), develops in the center of the system. The central superfluid phase grows with increasing number of particles, and the quasicondensate there becomes the highest populated. Finally, degeneracy sets up once again when the full filled insulator ($n = 1$) appears in the center of the trap [like in Fig. 11(d)].

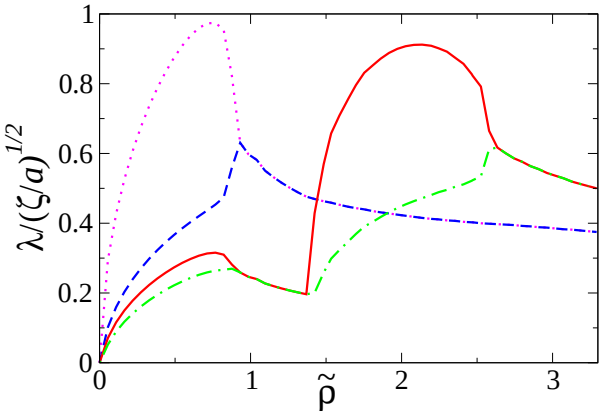

FIG. 14: (Color online) Occupations of the lowest 4 natural orbitals as a function of the characteristic density. These systems have 1000 lattice sites, $V_2a^2 = 3 \times 10^{-5}t$, $L = 2$, and $A = 0.5t$. Degeneracy sets in when insulating domains (with density $n = 0.5$ first and $n = 1.0$ second) appear in the middle of the trap.

V. DYNAMICS AND RELAXATION IN A HARMONIC TRAP

In this section we study the dynamics in the presence of a harmonic trap. Since at very low densities in the trap, when the average interparticle distance is much larger than the lattice spacing, the lattice system and the continuum are equivalent, we start analyzing this case.

We perform a numerical experiment similar to that recently done at Penn State [17]. There, in order to generate a highly exited state in a trap, an optical lattice potential was applied during a short period of time to an array of 1D Bose gases. This produced a momentum distribution with extra peaks away from $k = 0$ (the only one present in the absence of a lattice). After turning off the lattice potential the dynamics of the system was studied using time-of-flight measurements. It was

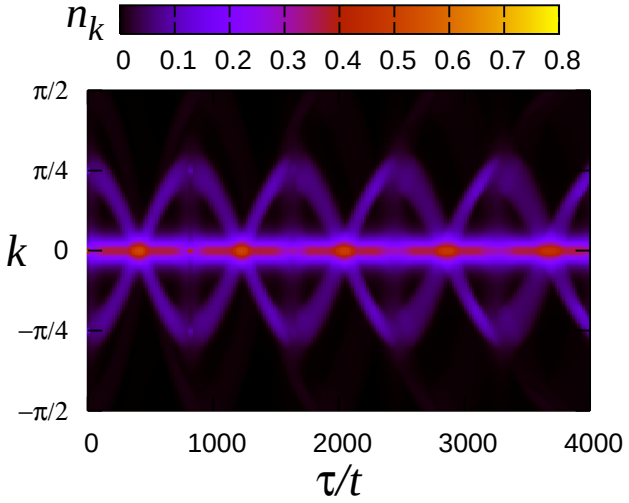

FIG. 15: (Color online) Evolution of the momentum distribution function after a superlattice potential with $L = 8$ and $A = 2.0t$ is applied for a short period of time ($\Delta\tau = 0.5t$) to the ground state of trapped system with 10 HCB's, $V_2a^2 = 4 \times 10^{-6}t$, and 2000 lattice sites. Undamped oscillations can be seen in n_k during our simulation time.

found that after some periods of oscillation the system relaxed to a momentum distribution that was not the one in thermal equilibrium. Relaxation to an equilibrium distribution was attributed mainly to the effects of the anharmonicity of the confining potential. In Ref. [18] and in this paper, we have shown why in the integrable limit of infinitely strong interactions the system relaxes to a distribution that is not the one in thermal equilibrium. Surprisingly, in the experiments [17] it was found that the absence of thermalization extends towards the nonintegrable region of finite interactions. Even though these 1D systems can be very well described by the Lieb-Liniger model [15], which is integrable in periodic homogeneous systems, the presence of the trapping potential in the experiment breaks integrability but did not allow the system to thermalize.

To recreate the experiment in Ref. [17] (performed in continuous space) in a perfect harmonic potential, we consider a very dilute system in our lattice model. We study the dynamics of 10 HCB's in 2000 lattice sites; i.e., the interparticle distance is much larger than the lattice spacing so that the effects of the underlying lattice are negligible. We then turn on, for a short period of time, an additional periodic potential with $L = 8$. The dynamics of the momentum distribution function after turning off this additional lattice is shown in Fig. 15. This figure shows that no relaxation towards an equilibrium distribution can be seen in the perfectly harmonic case. The additional peaks in n_k oscillate back and forth almost without damping. This occurs even when many eigenmodes of the system have been excited by turning on and off the lattice potential. Our results confirm the conclusion in Ref. [17] that relaxation in the hard-core regime may be mainly related to the anharmonicity of

the confining potential.

While the low-energy region (low occupation) of the harmonic trap spectrum in the presence of the lattice is like the one in the continuum, this is not true anymore in the high-energy region (high occupation); i.e., the lattice model and the continuum one start to differ [38, 60]. The spectrum in the lattice departs from the linear dispersion relation of the harmonic potential, and degeneracies set in when insulating domains develop in the ground state [61]. Hence, for large fillings in the trap we may expect to see relaxation towards an equilibrium distribution.

We study the dynamics of systems in which initially, in the presence of a superlattice potential, there is a coexistence of superfluid and insulating domains. We then turn off the superlattice potential and let the system evolve in the presence of the trap. In Fig. 16 we show the evolution of the occupations of the zero-momentum state ($n_{k=0}$) and the lowest natural orbital (λ_0) when (a) the initial state has a half-filled insulator in the center of the trap [Fig. 17(a)] and (b) two insulating shoulders surround a central superfluid region [Fig. 17(d)]. Figure 16 shows that for high fillings there is a strong damping of the oscillations of $n_{k=0}$ and λ_0, in contrast to the harmonically trapped case without the lattice. Hence, in experiments relaxation to an equilibrium state is to be expected when a lattice is present along the 1D tubes.

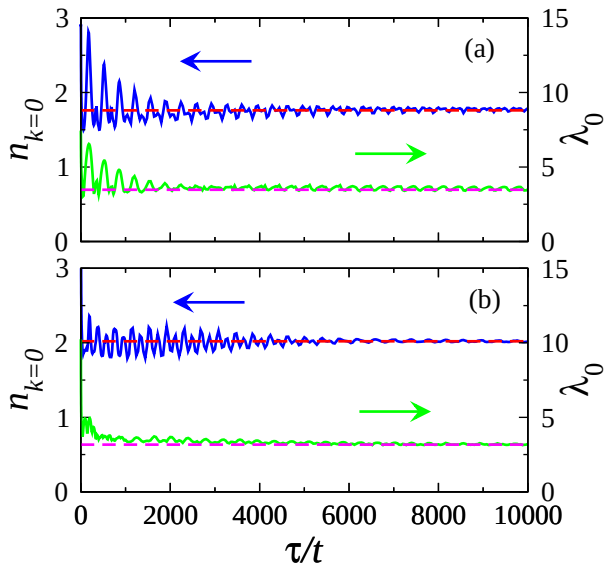

FIG. 16: (Color online) Evolution of the occupation of the zero-momentum state (top plots) and the occupation of the lowest natural orbital (bottom plots) after a superlattice potential is turned off in trapped systems with 900 lattice sites and $V_2a^2 = 3 \times 10^{-5}t$. The evolution starts from the ground state of a system with $L = 2$ and $A = 0.5t$. The number of particles is $N_b = 200$ (a) and $N_b = 299$ (b). The corresponding initial density profiles can be seen in Figs. 17(a) and 17(d). The dashed lines are the results obtained with the generalized Gibbs distribution explained in the text.

As seen in Fig. 16 after $\tau = 5000t$ the oscillations of $n_{k=0}$ and λ_0 are very small and occur around an approximately constant value. In Fig. 17, we compare the time average (between $\tau = 5000$ and $10000t$) of the density profiles, the momentum distribution function, and the natural orbitals, with the predictions of the usual grand-canonical ensemble and the generalized Gibbs distribution introduced in Ref. [18]. For all quantities the results of the time averages and the generalized Gibbs distribution are on top of each other. On the other hand, the differences between time averages and the thermal ensemble are apparent in all cases and particularly large in the low-momentum region of n_k and in the occupation of the lowest natural orbitals. Only in the density profiles are the differences smaller and mainly visible in the regions where the density approaches zero.

Since the density profiles of HCB's and noninteracting fermions are identical and their time average coincides with the results of the generalized Gibbs distribution, one realizes that noninteracting systems are the simplest case to which the constrained thermal equilibrium theory [18] explained in Sec. III can be applied.

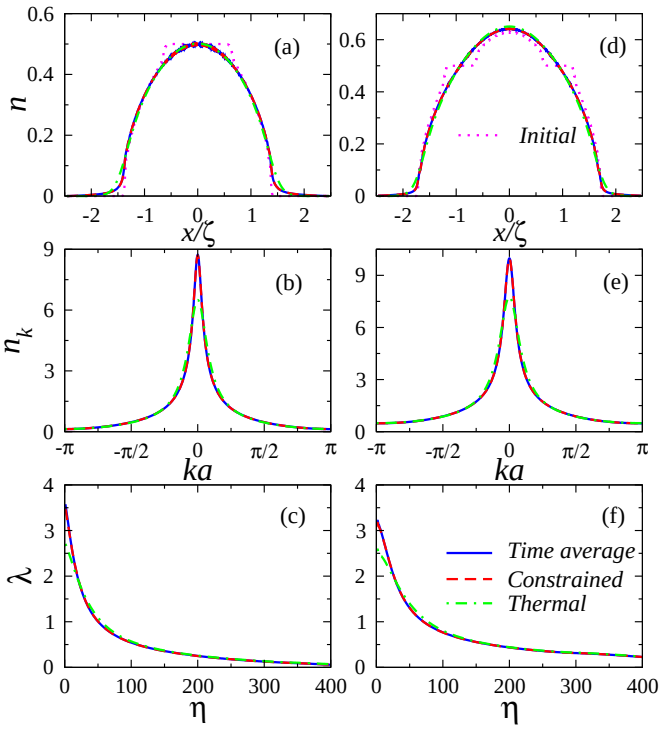

FIG. 17: (Color online) Time average of the density profiles (a),(d), momentum distribution function (b),(e), and the occupation of the lowest 400 natural orbitals. The average is performed between $\tau = 5000t$ and $\tau = 10000t$ (see Fig. 16) with measurements done in time intervals $\Delta\tau = 40t$. The evolution is performed in trapped systems with 900 lattice sites, $V_2a^2 = 3 \times 10^{-5}t$, starting from the ground state in the presence of a superlattice with $L = 2$ and $A = 0.5t$, after turning off the superlattice. The results of the time average are compared with the ones obtained in the usual thermal ensemble and the constrained theory explained in the text. The number of particles is $N_b = 200$ (a)–(c) and $N_b = 299$ (d)–(f). In (a) and (d) we included the averaged density per unit cell in the initial state. Flat regions correspond to insulating domains.

VI. CONCLUSIONS

We have studied ground-state properties and the nonequilibrium dynamics of hard-core bosons on one-dimensional lattices in the presence of an additional periodic potential (superlattice) and a harmonic trap.

In the periodic case the superlattice potential opens gaps at the borders of the reduced Brillouin zones generating insulating phases with fractional fillings. In these insulating phases one-particle correlations decay exponentially [$\rho_x \sim \exp(-x/\xi)$], and we have studied how the correlation length ξ behaves as a function of the strength A of the superlattice potential. On the other hand, we find that in the gapless superfluid phases one-particle correlations exhibit quasi-long-range order. They decay with the same power law shown in Ref. [38] to be universal in the absence of the superlattice potential.

In the presence of an additional confining potential, which we have taken to be harmonic for a closer connection to the experiments, superfluid and insulating domains coexist phase separated. We have shown that in the superfluid domains, where the density changes spatially, one-particle correlations decay with the same power law than in the homogeneous periodic case. This decay produces a square-root scaling of the occupation of the lowest natural orbital with the number of particles in the trap and independently of the presence or not of insulating domains.

We have also studied the nonequilibrium dynamics of these systems after a quench of the superlattice potential A. In particular, we have considered a half-filled box in the presence of a superlattice with period 2, since for $A = 0$ the system is superfluid while for $A \neq 0$ it is insulating. After a sudden switch-on of A we have shown that the initial momentum distribution (n_k) of the superfluid phase collapses and revives with a period determined by A, like in the experiment in Ref. [50] where the period was determined by the on-site repulsion U. After several oscillations, the number depending on A and the hopping parameter t, we have also seen that the system relaxes to an equilibrium distribution with very small fluctuations in n_k. The time average of this physical observable was then shown to be very well described by a generalized Gibbs distribution introduced in Ref. [18]. On the other hand, after a sudden switch-off of A we have found that not only the generalized Gibbs ensemble but also the usual thermal ensemble describes very well the time average result when the system is initially deep in the insulating regime ($A > t$). This is indeed a surprising result since we are seeing thermalization in an integrable system. But of course it is only seen in the very particular case in which the quench of the interaction drives the system from an insulating state to a superfluid one. In the latter the temperature plays a very similar role than the gap present in the initial insulator. In transitions between different superfluid states [18] no such thermalization is seen.

Finally, we have considered the nonequilibrium dynamics for the harmonically confined case. We have shown that in this more experimentally relevant system the time average of observables, like density and momentum distribution, can also be very well described by the generalized Gibbs distribution. Damping occurs in this case, even in a perfect harmonic trap, because of the presence of the lattice. At very low densities, equivalent to the continuum case, we have shown that oscillations of n_k occur almost without damping.

Acknowledgments

We would like to thank the Max Planck Institute for the Physics of Complex Systems in Dresden for the hospitality during the "Workshop on Non-equilibrium Dynamics in Interacting System" where this work was initiated. We acknowledge stimulating conversations during the workshop with M. A. Cazalilla, C. Kollath, A. Kolovsky, S. Manmana, D. Weiss, and X. Zotos. We are also grateful to R. T. Scalettar and R. R. P. Singh for helpful discussions. This work was supported by National Science Foundation grants Nos. NSF-DMR-0240918, NSF-DMR-0312261, NSF-PHY-0301052, a grant from Office of Naval Research No. N00014-03-1-0427, and SFB/TR 21 and HLR-Stuttgart in Germany.

[1] http://www.mpipks-dresden.mpg.de/∼neqdis06/
[2] J. H. Thywissen, R. M. Westervelt, and M. Prentiss, Phys. Rev. Lett. **83**, 3762 (1999).
[3] D. Müller, D. Z. Anderson, R. J. Grow, P. D. D. Schwindt, and E. A. Cornell, Phys. Rev. Lett. **83**, 5194 (1999).
[4] N. H. Dekker, C. S. Lee, V. Lorent, J. H. Thywissen, S. P. Smith, M. Drndic, R. M. Westervelt, and M. Prentiss, Phys. Rev. Lett. **84**, 1124 (2000).
[5] M. Key, I. G. Hughes, W. Rooijakkers, B. E. Sauer, E. A. Hinds, D. J. Richardson, and P. G. Kazansky, Phys. Rev. Lett. **84**, 1371 (2000).
[6] K. Bongs, S. Burger, S. Dettmer, D. Hellweg, J. Arlt, W. Ertmer, and K. Sengstock, Phys. Rev. A **63**, 031602(R) (2001).
[7] F. Schreck, L. Khaykovich, K. L. Corwin, G. Ferrari, T. Bourdel, J. Cubizolles, and C. Salomon, Phys. Rev. Lett. **87**, 080403 (2001).
[8] A. Görlitz, J. M. Vogels, A. E. Leanhardt, C. Raman, T. L. Gustavson, J. R. Abo-Shaeer, A. P. Chikkatur, S. Gupta, S. Inouye, T. Rosenband, and W. Ketterle, Phys. Rev. Lett. **87**, 130402 (2001).
[9] K. E. Strecker, G. B. Partridge, A. G. Truscott, and R. G. Hulet, Nature (London), **417**, 150 (2002).
[10] M. Greiner, I. Bloch, O. Mandel, T. W. Hänsch, and T. Esslinger, Phys. Rev. Lett. **87**, 160405 (2001).

[11] H. Moritz, T. Stöferle, M. Köhl, and T. Esslinger, Phys. Rev. Lett. **91**, 250402 (2003).
[12] T. Stöferle, H. Moritz, C. Schori, M. Köhl, and T. Esslinger, Phys. Rev. Lett. **92**, 130403 (2004).
[13] B. L. Tolra, K. M. O'Hara, J. H. Huckans, W. D. Phillips, S. L. Rolston, and J. V. Porto, Phys. Rev. Lett. **92**, 190401 (2004).
[14] B. Paredes, A. Widera, V. Murg, O. Mandel, S. Fölling, I. Cirac, G. V. Shlyapnikov, T. W. Hänsch, and I. Bloch, Nature (London) **429**, 277 (2004).
[15] T. Kinoshita, T. Wenger, and D. S. Weiss, Science **305**, 1125 (2004).
[16] C. D. Fertig, K. M. O'Hara, J. H. Huckans, S. L. Rolston, W. D. Phillips, and J. V. Porto, Phys. Rev. Lett. **94**, 120403 (2005).
[17] T. Kinoshita, T. Wenger, and D. S. Weiss, Nature (London) **440**, 900 (2006).
[18] M. Rigol, V. Dunjko, V. Yurovsky, and M. Olshanii, e-print cond-mat/0604476.
[19] F. Iglói and H. Rieger, Phys. Rev. Lett. **85**, 3233 (2000).
[20] K. Sengupta, S. Powell, and S. Sachdev, Phys. Rev. A **69**, 053616 (2004).
[21] P. Calabrese and J. Cardy, Phys. Rev. Lett. **96**, 136801 (2006).
[22] R. W. Cherng and L. S. Levitov, Phys. Rev. A **73**, 043614 (2006).
[23] M. A. Cazalilla, Phys. Rev. Lett. **97**, 156403 (2006).
[24] M. Olshanii, Phys. Rev. Lett. **81**, 938 (1998).
[25] D. S. Petrov, G. V. Shlyapnikov, and J. T. M. Walraven, Phys. Rev. Lett. **85**, 3745 (2000).
[26] V. Dunjko, V. Lorent, and M. Olshanii, Phys. Rev. Lett. **86**, 5413 (2001).
[27] M. Girardeau, J. Math. Phys. **1**, 516 (1960).
[28] M. D. Girardeau and E. M. Wright, Phys. Rev. Lett. **84**, 5691 (2000).
[29] M. D. Girardeau and E. M. Wright, Phys. Rev. Lett. **84**, 5239 (2000).
[30] K. K. Das, M. D. Girardeau, and E. M. Wright, Phys. Rev. Lett. **89**, 170404 (2002).
[31] A. Minguzzi and D. M. Gangardt, Phys. Rev. Lett. **94**, 240404 (2005).
[32] A. del Campo and J. G. Muga, Europhys. Lett. **74**, 965 (2006).
[33] E. Lieb, T. Shultz, and D. Mattis, Ann. Phys. (N.Y.) **16**, 407 (1961).
[34] B. M. McCoy, Phys. Rev. **173**, 531 (1968).
[35] H. G. Vaidya and C. A. Tracy, Phys. Lett. **68**A, 378 (1978).
[36] B. M. McCoy, J. H. Perk, and R. E. Schrock, Nucl. Phys. B **220**, 35 (1983); **220**, 269 (1983).
[37] D. M. Gangardt and G. V. Shlyapnikov, New J. Phys. **8** 167 (2006).
[38] M. Rigol and A. Muramatsu, Phys. Rev. A **70**, 031603(R) (2004); **72**, 013604 (2005).
[39] M. Rigol and A. Muramatsu, Phys. Rev. Lett. **93**, 230404 (2004).
[40] M. Rigol and A. Muramatsu, Phys. Rev. Lett. **94**, 240403 (2005).
[41] M. Rigol and A. Muramatsu, Mod. Phys. Lett. B **19**, 861 (2005).
[42] S. Peil, J. V. Porto, B. L. Tolra, J. M. Obrecht, B. E. King, M. Subbotin, S. L. Rolston, and W. D. Phillips, Phys. Rev. A **67**, 051603(R) (2003).
[43] J. Sebby-Strabley, M. Anderlini, P. S. Jessen, and J. V. Porto, Phys. Rev. A **73**, 033605 (2006).
[44] P. Buonsante and A. Vezzani, Phys. Rev. A **70**, 033608 (2004); P. Buonsante, V. Penna, and A. Vezzani, *ibid.* **70**, 061603(R) (2004); P. Buonsante and A. Vezzani, *ibid.* **72**, 013614 (2005).
[45] V. G. Rousseau, D. P. Arovas, M. Rigol, F. Hébert, G. G. Batrouni, and R. T. Scalettar, Phys. Rev. B **73**, 174516 (2006).
[46] A. M. Rey, I. I. Satija, and C. W. Clark, New J. Phys. **8**, 155 (2006).
[47] M. Aizenman, E. H. Lieb, R. Seiringer, J. P. Solovej, and J. Yngvason, Phys. Rev. A **70**, 023612 (2004).
[48] P. Jordan and E. Wigner, Z. Phys. **47**, 631 (1928).
[49] M. Rigol, Phys. Rev. A **72**, 063607 (2005).
[50] M. Greiner, O. Mandel, T. W. Hänsch, and I. Bloch, Nature (London) **419**, 51 (2002).
[51] G. G. Batrouni, V. Rousseau, R. T. Scalettar, M. Rigol, A. Muramatsu, P. J. H. Denteneer, and M. Troyer, Phys. Rev. Lett. **89**, 117203 (2002).
[52] C. Kollath, U. Schollwöck, J. von Delft, and W. Zwerger, Phys. Rev. A **69**, 031601(R) (2004).
[53] S. Wessel, F. Alet, M. Troyer, and G. G. Batrouni, Phys. Rev. A **70**, 053615 (2004).
[54] O. Penrose and L. Onsager, Phys. Rev. **104** 576, (1956).
[55] A. J. Leggett, Rev. Mod. Phys. **73**, 307 (2001).
[56] C. N. Yang, Rev. Mod. Phys. **34**, 694 (1962).
[57] T. Papenbrock, Phys. Rev. A **67**, 041601(R) (2003).
[58] P. J. Forrester, N. E. Frankel, T. M. Garoni, and N. S. Witte, Phys. Rev. A **67**, 043607 (2003).
[59] D. M. Gangardt, J. Phys. A **37**, 9335 (2004).
[60] M. A. Cazalilla, Phys. Rev. A **70**, 041604(R) (2004).
[61] M. Rigol and A. Muramatsu, Phys. Rev. A **70**, 043627 (2004).